Journal of Solid State Chemistry **166,** 375–381 (2002)
doi:10.1006/jssc.2002.9608

Structure Investigation and Electrochemical Behavior of γ-MnO_2 Synthesized from Three-Dimensional Framework and Layered Structures

Kh. S. Abou-El-Sherbini[1]

Inorganic Chemistry Department, National Research Center, 31 Tahrir Street, Dokki, Giza, Egypt

Received January 2, 2002; in revised form March 23, 2002; accepted April 5, 2002

MnO_2 was chemically prepared from birnessite (CMD_{2D}) and from spinel-like $LiMn_2O_4$ (CMD_{3D}) by acid leaching. X-ray diffractometry, FTIR spectrometry, chemical and thermal analyses were used to determine the structure and chemical disorder. On the basis of cation vacancy model, the structural water was found to be mainly due to Coleman protons in both samples. Both samples were found to be of very close structure belonging to γ-MnO_2 type I according to Chabre and Pannetier classification with de Wolff disorder (P_r) of 0.19 and 0.30 and microtwinning (Tw) of 9.9 and 17%, respectively. The activation energy of structural water release calculated from thermal analysis was apparently higher than that of other γ-MnO_2 types (150 and 156.6 kJ/mol, respectively).

A high reduction capacity in aqueous and non-aqueous batteries was delivered for both samples except for the electrochemical lithium insertion of CMD_{2D}, which was attributed to the different oxygen packing. © 2002 Elsevier Science (USA)

Key Words: **chemically prepared γ-MnO_2; structural composition; de Wolff disorder; microtwinning; cation vacancy model; electrochemical behavior.**

INTRODUCTION

Manganese dioxide is rich with different allotropic polymorphs denoted by $\alpha, \beta, \gamma, \varepsilon, \lambda, \delta$, etc. which differ in the way of distribution of Mn ions in the octahedral sites of hcp or ccp arrays of oxygen network (1). Two main types of structures have been identified: three-dimensional (3D) octahedral framework such as hollandite (2–4), cryptomelane (2), pyrolusite (5), ramsdellite (6), nsutite (7) and spinel-like λ-MnO_2 (8–10); and two-dimensional (2D) layered structures such as phyllomanganate, birnessite, buserite and chalcophanite (11–13). These modifications are characterized by their ability to accommodate different ions depending on the size of the available site. Another interesting feature of these MnO_2 modifications is the possibility of their transformation to each other by the redistribution of Mn ions within the oxygen network as described in Fig. 1. From this figure, δ-MnO_2 appears to be an important precursor to obtain different MnO_2 modifications (14–21). Also, another observation is the transformation of different modifications to the spinel-like $LiMn_2O_4$ upon thermal treatment in the presence of Li.

γ-MnO_2, which is popular as cathodic material for primary batteries, was described by de Wolff (7) as random intergrowth of β-MnO_2 layers in a ramsdellite matrix.

A major step in the chemical understanding of γ-MnO_2 was achieved when Ruetschi (22) and Ruetschi and Giovanoli (23) demonstrated that its chemical composition and density could be explained by assuming a cation vacancy model namely that non-stoichiometry is found only on the cationic lattice. For charge compensation, each of the Mn^{4+} vacancies in coordination with four protons in the form of OH^- anions at the sites of the O^{2-} ions, result in the so-called structural water.

Recently, Chabre and Pannetier (24) succeeded in correlating the electrochemical behavior with the structure by suggesting two kinds of structural defects in an idealized ramsdellite host structure. The first type is a random planner fault based on the model originally constructed by de Wolff (P_r). The second type was identified as microtwinning (Tw) of the orthorhombic ramsdellite-type lattice on the 021 and/or 061 planes. Moreover, this model explains, in particular, the poor quality of powder X-ray diffractograms of most γ-MnO_2's which led to its classification into four types according to the degree of P_r and Tw.

In a previous work (25), five samples belonging to γ-MnO_2 types II–IV in the Chabre and Pannetier scheme (24) were examined in accordance with this model and also the cation vacancies Ruetschi's model (22, 23). It was recom-

[1] To whom correspondence should be addressed. Fax: +20-2-3370931. E-mail: kh_sherbini@yahoo.com.

0022-4596/02 $35.00

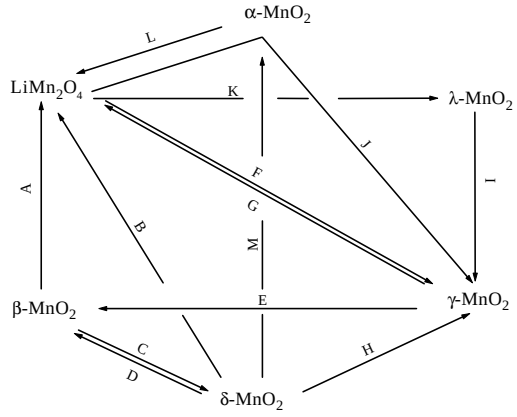

FIG. 1. Schematic representation of the phase transformations between different manganese dioxides modifications, phyllomanganate, and lithium manganate. (A) Heating at 700°C with 0.5 M LiOH for 24 h under N_2 (21) or heat treatment after lithiation with LiI (20); (B) hydrothermal treatment of Li-birnessite (4); (C) hydrothermal treatment with 20M NaOH followed by hydration (19); (D) hydrothermal treatment of Mg-birnessite with 0.5M H_2SO_4, 1M $MgCl_2$ (4); (E) reflux with 1M H_2SO_4 for 24 h (14); (F) digestion in 2.5 M H_2SO_4 at 95°C for 24 h (15,17); (G) heat treatment after lithiation with LiI (20); (H) prolonged acid treatment of Na-phase (18,19) or hydrothermal treatment of Li-phase with 0.5M H_2SO_4, 1M LiCl (4); (I) digestion in 2.5 M H_2SO_4 at 95°C for 24 h (17); (J) digestion in 2.5M H_2SO_4 at 95°C for 24 h and step-transformation to γ-MnO_2 via α-MnO_2 (17); (K) acid treatment at room temperature (16); (L) heat treatment after lithiation with LiI (20); (M) hydrothermal treatment of K- or Ba-birnessite (3,4).

mended that a γ-MnO_2 type-III sample (denoted EMD2) is a promising cathodic material as it acquires maximum value of Tw ($>80\%$) and minimum values of P_r (0.31) and activation energy of structural water release (68 kJ/mol). As a continuation, the present work aims to compare the structural and electrochemical behavior of γ-MnO_2 type I synthesized by phase transformation from the (2D) birnessite and from the (3D) spinel-like $LiMn_2O_4$ in view of the cation vacancy and Chabre and Pannetier models.

EXPERIMENTAL

Na-birnessite was synthesized by precipitating $Mn(OH)_2$ from $Mn(NO_3)_2$ by adding NaOH at <5°C, then O_2 was bubbled overnight through a glass frit G1 (11, 12). The black product was washed with water until pH 7 and dried in air at room temperature.

CMD_{2D} was synthesized according to the literature (26) by treatment of Na-birnessite with 0.05 M H_2SO_4 solution for 40 days with daily decantation and addition of fresh acid. The product was washed with water until pH 7 and dried at 200°C for 2 h.

Spinel-like phase, $LiMn_2O_4$ was synthesized by mixing $LiOH \cdot H_2O$ and β-MnO_2 in the ratio 1:2 in ball-mortar for 2 h, then pressed into pellets under 10 t/cm^2, and heated at 470°C for 24 h in air and at 700°C for 12 h under N_2 (21).

CMD_{3D} was synthesized by refluxing $LiMn_2O_4$ with 2.5 M H_2SO_4 at 95°C for 24 h. The product was washed with distilled water to pH 7 and dried at 200°C for 2 h.

Electrolytically prepared MnO_2, MOL85Ti, was kindly provided by Prof. R. Schöllhorn, Institut für Anorganische und Analytische Chemie, Technische Universität Berlin.

The samples were characterized by chemical, powder X-ray diffraction and thermogravimetric analyses.

Chemical analysis. The available oxygen as MnO_2 and the total manganese in the prepared samples were determined by the standard iodometry and atomic absorption spectrometry, respectively. Structural water was determined from the weight loss in the temperature range 150–400°C (23). The chemical formulae were calculated on the basis of cation vacancy model (22, 23) and represented by

$$Mn^{4+}_{(1-x-y)}Mn^{3+}_{y}O^{2-}_{(2-4x-y)}OH^{-}_{(4x+y)},$$

where x is the fraction of Mn^{4+} missed from the MnO_2 lattice resulting in Mn vacancies; y is the fraction of Mn^{4+} replaced by Mn^{3+}, and calculated by the set of equations

$$x = \frac{m}{2+m} \quad [1]$$

$$y = \frac{4(2-n)}{2+m} \quad [2]$$

and are calculated from knowing n and m in the general formula

$$MnO_n \cdot (2-n+m)H_2O,$$

where n is the degree of oxidation ($2n$ = average Mn valency), $(2-n+m)$ represents the total structural water and m represents the neutral water.

X-ray diffractometry (XRD). For structural investigations, a powder diffractometer (Siemens D5000) was used with Cu$K\alpha$ radiation ($2\theta = 10-70°$, $\lambda = 1.5406$ Å, 30 kV and 8 mA). For the lattice parameters refinement, a commercial regression program was used. As a standard, quartz was used for calibration. The refinement was performed on a selection of lines with $k/2+1$ even (namely (021), (121), (140), (221), (240) and (002)) which are not affected by de Wolff disorder (P_r) whereas they are equally affected by microtwinning (Tw). The amounts of microtwinning and de Wolff disorders were evaluated according to the scheme given by Chabre and Pannettier (24). Tw was calculated by applying the linear equation

$$\mathrm{Tw} = 871\left(\frac{b}{2c}\right) - 1409, \quad [3]$$

whereas P_r was determined from the shift of the 110 line corrected for microtwinning contribution.

Thermogravimetric analysis. An automatic recording thermobalance type (951 Dupant instrument) was used in this study. The samples were subjected to heat using a rate of heating 10°C/min from room temperature to 1000°C in air. The activation energy of structural water removal was calculated based on Chatterjee's method (27).

IR absorption spectra were recorded using Mattson 5000 FTIR spectrometer for a sample of 2–3 mg diluted with 300 mg KBr and pressed into tablet under 10 t/cm^2.

Electrochemical reactions were performed in three-electrode cells with commercial potentiostat. In galvanostatic processes, a current density of 5 mA/g was used. Hg/HgO and Pt sheet were used as reference and counter-electrodes, respectively, in aqueous electrolyte whereas Li metal was used as both counter and reference electrodes in non-aqueous electrolyte. The working electrodes were pressed tablets under 3 t/cm^2 in platinum-grid-pressed powder electrodes, with 50% (wt/wt) graphite (KS6 from LONZA) in respect to manganese dioxide samples and ca. 1% (wt/wt) PTFE.

Aqueous 1 M KOH was used as electrolyte in H^+/e^- insertion study. In the case of lithium insertion study, 1 M lithium trifluoromethane sulfonate $LiCF_3SO_3$ (Fluka) (dried by heating at 80°C under vacuum for 12 h) dissolved in propylene carbonate (Merck) (dried by 3 Å mol. sieve from Metrohm) and kept with extra amount of the mol. sieve under dry oxygen-free argon atmosphere in glove box was used as electrolyte.

TABLE 1
Preparation, Chemical Analysis and Ruetschi's Chemical Formulae of γ-MnO_2 Samples

Sample	CMD_{2D}	CMD_{3D}
Starting material	Na-birnessite	$LiMn_2O_4$
Leaching solution, temperature, time	0.05 M H_2SO_4, 25°C, 40 days	2.5 M H_2SO_4, 95°C, 24 h
MnO_2, $\bar{X}\pm ts/\sqrt{n}$ %	84.43±1.19	88.26±1.22
Mn, $\bar{X}\pm ts/\sqrt{n}$ %	62.04±0.72	62.12±0.66
Adsorbed water, %	1.67	1.47
Combined water, % (H_2O/Mn)	1.43	1.16
	(0.070)	(0.057)
n	1.930	1.949
m	0.000	0.006
x	0.000	0.003
y	0.140	0.102
Formula	$Mn^{4+}_{0.860}Mn^{3+}_{0.140}O^{2-}_{1.860}$ $OH^-_{0.140}$	$Mn^{4+}_{0.895}Mn^{3+}_{0.102}O^{2-}_{1.886}$ $OH^-_{0.114}$

Note. $\bar{X}$ = average value, $n = 5$, s = standard deviation, t = Student's factor, $P = 0.05$.

RESULTS AND DISCUSSION

Chemical Analysis

Table 1 shows the results of chemical analysis of CMD_{2D} and CMD_{3D}. The degree of oxidation (n) of CMD_{3D} was comparable to that reported earlier (28) whereas the water content was slightly lower due to the heat treatment. The degree of oxidation of CMD_{2D} was relatively lower than CMD_{3D} due to the use of more powerful leaching solution of the latter. Both samples show lower values of structural water when compared with γ-MnO_2 types III and IV (25). Ruetschi's parameter x value was almost zero in both samples indicating a negligible amount of Mn vacancies. This means that most protons contained in the lattices of CMD_{2D} and CMD_{3D} are present in conjunction with Mn^{3+} ion, which is called Coleman protons (23).

Structural Characterization

The X-ray diffraction patterns of the investigated samples are shown in Fig. 2. Birnessite and spinel-like $LiMn_2O_4$ showed XRD patterns typical to PDF nos. 43-1456 and 35-782, respectively. The diffractograms of CMD_{2D} and CMD_{3D} indicates that both samples belong

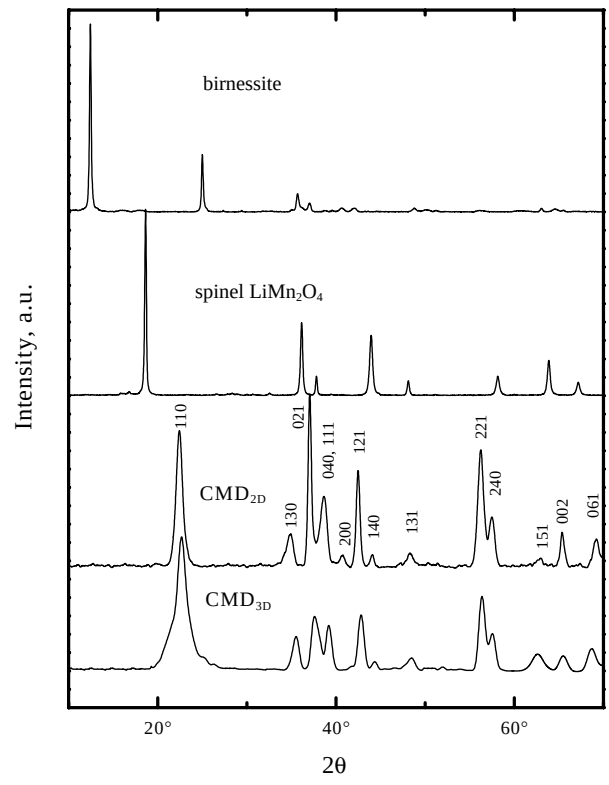

FIG. 2. XRD patterns of γ-MnO_2 phases CMD_{2D} and CMD_{3D} obtained by acid leaching of birnessite and spinel-like $LiMn_2O_4$, respectively.

TABLE 2
Lattice and Chabre and Pannetier Parameters Obtained from X-Ray Diffraction Measurements

Parameter	Sample			
	CMD_{2D}	CMD_{3D}	S-ramsdellite	Synthetic ramsdellite from Thackeray
Cell parameters, Å	$a = 4.447$	$a = 4.476$	$a = 4.4785$	$a = 4.499$
	$b = 9.336$	$b = 9.283$	$b = 9.3547$	$b = 9.3607$
	$c = 2.865$	$c = 2.835$	$c = 2.8537$	$c = 2.8459$
Volume, $Å^3$	118.972	117.789	119.556	119.852
R	0.038	0.047	—	—
Type	I	I	I	I
Tw, %	9.9	17	20	25
P_r	0.19	0.30	0.20	0.27
Reference	This work	This work	28	28

to γ-MnO_2 type I as they show splitting of the 221/240 and 002/061 reflections indicating $Tw < 50\%$ according to Chabre and Pannetier classification (24). The lattice and the Chabre and Pannetier parameters (P_r and Tw) are presented in Table 2. These values are generally comparable to those reported for synthetic ramsdellite obtained by hot acid leaching of spinel-like $LiMn_2O_4$ (28). The b and c values of CMD_{3D} were significantly lower than the reported values due to the high drying temperature (200°C) which was used to minimize the amount of physically adsorbed water. CMD_{2D} also showed significantly lower Tw value, which may be attributed to three reasons: (I) the slow room-temperature acid-leaching procedure may enable better rearrangement of the birnessite to the ramsdellite phase; (II) the birnessite phase acquires minimum ratio of Mn vacancies, which are correlated to Tw (24), as low as 1:15 with respect to the filled MnO_6 (13); and (III) the healing out of Mn vacancies due to drying at 200°C (23).

CMD_{2D} showed IR absorption bands at 476, 535, 570, 712, 1068 and 1633 cm^{-1} which are close to those detected for CMD_{3D} at 478, 518, 577, 706, 1061 and 1618 cm^{-1} (Fig. 3). The band positions in both samples are in agreement with those of nsutite reported earlier (29). The last band is attributed to the OH-bending mode of vibration.

Thermal Analysis

The thermogravimetric analysis of these samples up to 1000 (Fig. 4) showed a typical γ-MnO_2 behavior as four stages were detected (30). The first stage was from room

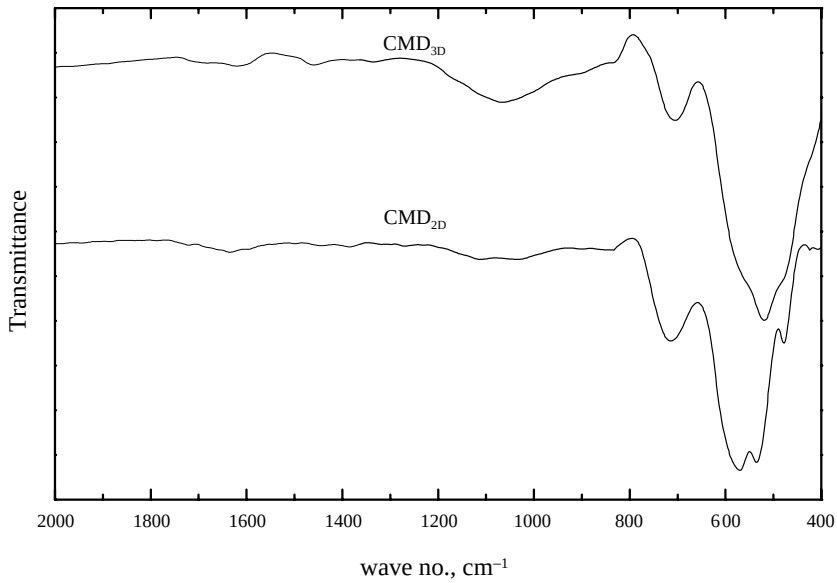

FIG. 3. IR absorption spectra of γ-MnO_2 phases CMD_{2D} and CMD_{3D}.

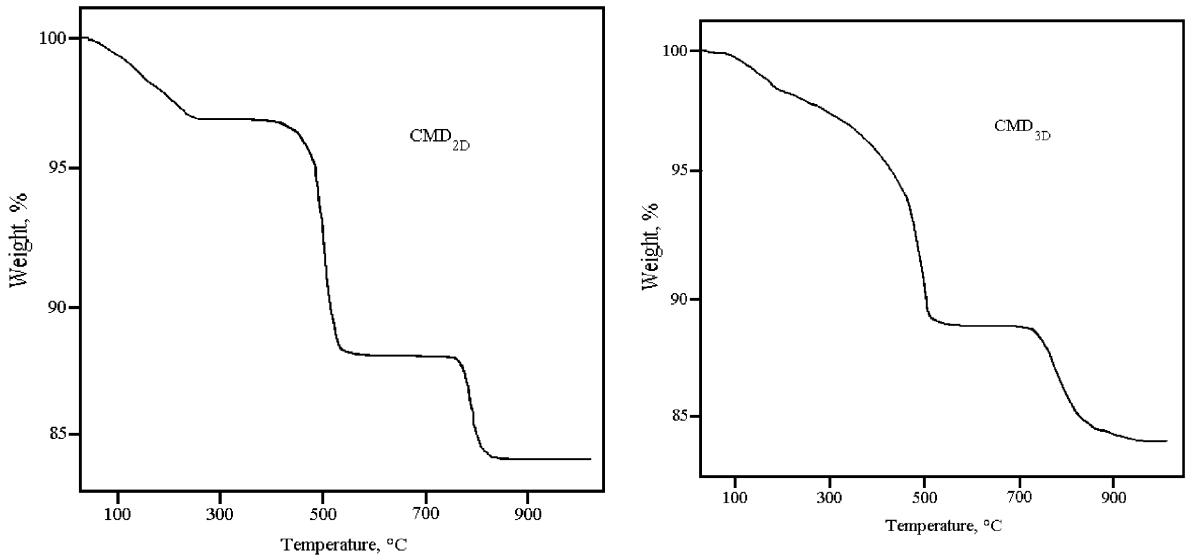

FIG. 4. Thermogravimetric curves of CMD_{2D} and CMD_{3D}.

temperature up to $\approx 180°C$ representing physically bonded water and the second stage was from 200 to 350°C and represented chemically bonded water. These two stages are representing the total amount of water in CMD_{2D} and CMD_{3D} (3.10 and 2.63%, respectively) which are in agreement with those reported by MacLean *et al.* (28) for synthetic ramsdellite type-I prepared from $LiMn_2O_4$. It is important to refer that no definite limit between the second and third stages for CMD_{3D} was observed. The third stage occur in the range 450–500°C which was due to the formation of Mn_2O_3 and the last stage took place from 750 to 800°C representing the transformation from Mn_2O_3 to Mn_3O_4.

In the temperature range between 200 and 400°C, the weight loss represents the removal of structural water (23). On the basis of cation vacancy model suggested by Ruetschi (22), all the structural water is present in the form of OH ions associated with either Mn vacancies (x) or Mn^{3+} (y) in the network of MnO_2. Removal of this structural water is due to healing out of cation vacancies and the oxidation of Mn^{3+} to Mn^{4+} in the presence of oxygen (from air). Thereby, Mn cations jump into vacant lattice positions and protons associated with vacancies diffuse to the surface of the crystal, where they combine with surplus O^{2-} to form water, which then evaporates. The calculated activation energy of the structural water release (E_a) in CMD_{2D} and CMD_{3D} were 150 and 156.6 kJ/mol, respectively. These values are apparently greater than those reported previously for γ-MnO_2 types II and III. This is attributed to the fact that the latter two types are more strongly disordered with P_r and Tw defects. Also, it was reported that the activation energy of structural water release decreases with increasing Ruetschi protons, x, (23), which is related to the Tw defect (24). As both Tw and x values are low in the investigated samples, they are expected to show high E_a.

Electrochemical Behavior

The galvanostatic reduction of CMD_{2D} and CMD_{3D} in aqueous 1 M KOH are presented in comparison with that of MOL85Ti (which was reported previously to be γ-MnO_2 type III, (25)) in Fig. 5 with a cut-off potential of -600 mV vs Hg/HgO. The discharge capacity of CMD_{2D} was close to that of CMD_{3D} (0.87 and 0.90 electron/formula unit, e^-/fu, respectively) but it was higher than that of MOL85Ti (0.79 e^-/fu). This agrees with the observation of Larcher *et al.* (17) who stated that it is not attributed to the different water content. It may be attributed to the fact that MOL85Ti has pyrolusite faults, $P_r = 0.37$ (25) (which cannot be reduced at the given pH through proton diffusion mechanism (24)) more than CMD_{2D} and CMD_{3D}, $P_r = 0.16$ and 0.20, respectively (Table 2). MOL85Ti also was observed to insert protons at higher potential than CMD_{2D} and CMD_{3D} which is in agreement with the previous results which may be attributed to its higher amount of microtwinning (Tw) which enhances the activity of manganese dioxide (25). As Chabre and Pannetier (24) related the amount of microtwinning to the amount of Ruetschi's protons (arose from Mn vacancies) which is directly proportional to E_a (22, 23), type-III γ-MnO_2 should acquire higher activity than type I which has a negligible amount of Ruetschi's protons.

The galvanostatic reduction of CMD_{2D} in 1 M $LiCF_3SO_3$/propylene carbonate (Fig. 6, solid line) with a

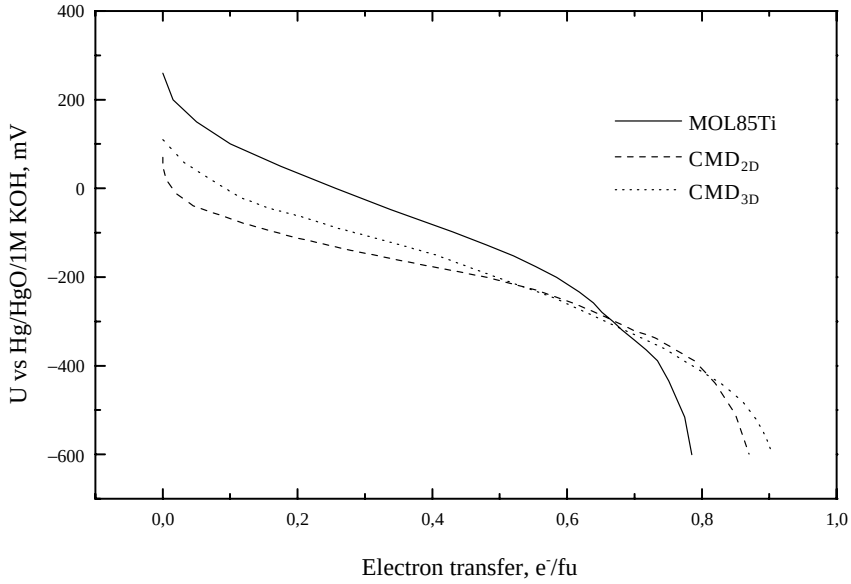

FIG. 5. Galvanostatic reduction of γ-MnO_2 phases MOL85Ti, CMD_{2D} and CMD_{3D} in 1 M KOH.

cut-off potential of 2 V vs Li/Li^+, delivered a capacity of 0.52 (e^-/fu) in two stages. In the case of CMD_{3D}, the galvanostatic reduction (Fig. 6, dashed line) delivered 0.59 e^-/fu which is lower than that of synthetic ramsdellite (0.72 e^-/fu) obtained by a similar method (15) which may be attributed to the application of higher current density. However, the two-step reduction was observed to be similar to that of CMD_{2D}. The first step in the reduction was 0.25 and 0.22 e^-/fu for CMD_{2D} and CMD_{3D} whereas the second step was 0.27 and 0.37 e^-/fu, respectively. These two steps were described by Thackeray *et al.* (15) as the first step is due to the insertion of lithium into the hexagonally close-packed (hcp) ramsdellite structure whereas the second step represents the insertion of lithium into ramsdellite framework structure in which the packing of the oxygen is ABACABAC. Consequently, an important difference between CMD_{2D} and CMD_{3D} may be concluded from the behavior in the first galvanostatic reduction, that the ABACABAC oxygen packing in the latter is apparently greater. This may be attributed to the fact that the starting phase in the case of CMD_{2D} (birnessite) has the hcp oxygen arrays (ABABAB) whereas in the case of CMD_{3D} the

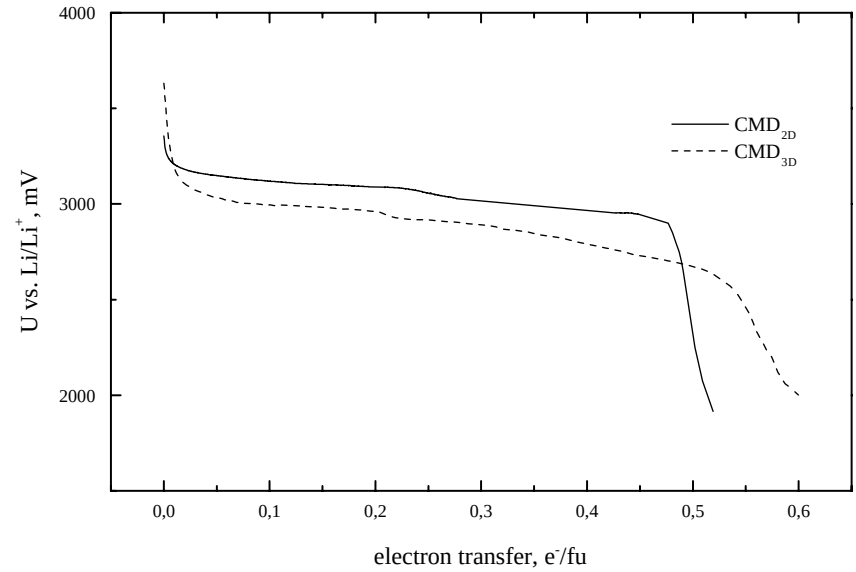

FIG. 6. Galvanostatic reduction of CMD_{2D} and CMD_{3D} in 1 M $LiCF_3SO_3$ dissolved in propylene carbonate.

starting phase is the spinel-like $LiMn_2O_4$ in which the oxygen framework is cubic-close-packed, ccp (ABCABC) (8).

CONCLUSION

From the chemical analysis, structure investigation, thermal analysis and electrochemical study, CMD_{2D} showed high similarity to CMD_{3D} indicating that both samples are of ramsdellite structure with a small amount of structural defects. Consequently, dilute sulfuric acid treatment of birnessite at room temperature may be considered as an alternative method for the preparation of highly crystalline synthetic ramsdellite with the minimum amount of lattice disorders.

Regarding the low values of de Wolff defect P_r in the investigated samples with respect to types II–IV, they are expected to show high cathodic capacity in dilute alkaline batteries and better lithium-ion diffusion in non-aqueous batteries. This was confirmed in the electrochemical study of both samples except for the electrochemical lithium insertion of CMD_{2D} which led to low discharge capacity in respect to that of CMD_{3D}. This may be attributed to the difference in the oxygen close packing in the parent structures, which affects the oxygen arrangement in the yielded ramsdellite phases.

REFERENCES

1. J. O. Besenhard, "Handbook of Battery Materials," pp. 85–133. Wiley/VCH Verlag Gmbh, Weinheim, Germany, 1999.
2. J. Post, R. Von Dreele, and P. Buseck, *Acta Crystallogr. B* **38,** 1056 (1982).
3. R. Giovanoli and B. Balmer, *Chimia* **35,** 53 (1981).
4. M. Rossouw, D. Liles, M. Thackeray, W. David, and S. Hull, *Mat. Res. Bull.* **27,** 221 (1992).
5. W. Baur, *Acta Crystallogr. B* **32,** 2200 (1976).
6. A. Byström, *Acta Chem. Scand.* **3,** 163 (1949).
7. P. De Wolff, *Acta Crystallogr.* **12,** 341 (1959).
8. M. Thackeray, *Prog. Solid State. Chem.* **25,** 1 (1997).
9. F. Cras, P. Strobel, M. Anne, D. Bloch, J.-B. Soupart, and J.-C. Rousche, *Eur. J. Solid State Inorg. Chem.* **33,** 67 (1996).
10. G. Pistoia, A. Antonini, D. Zane, and M. Pasquali, *J. Power Sources* **56,** 37 (1995).
11. P. Le Goff, N. Baffier, S. Bach, and J.-P. Pereira-Ramos, *Mater. Res. Bull.* **31,** 63 (1996).
12. P. Strobel, J.-C. Charenton, and M. Lenglet, *Rev. Chim. Minér.* **24,** 199 (1987).
13. J. Post and D. Veblen, Am. Mineral. **75,** 477 (1990).
14. W.-H. Kao, *J. Electrochem. Soc.* **136,** 13 (1989).
15. M. Thackeray, M. Rossouw, R. Gummow, D. Liles, K. Pearce, A. De Kock, W. David, and S. Hull, *Electrochim. Acta* **38,** 1259 (1993).
16. J. Hunter, *J. Solid State. Chem.* **39,** 142 (1981).
17. D. Larcher, P. Courjal, R. Herrera Urbina, B. Gérand, A. Blyr, A. du Pasquier, and J.-M. Tarascon, *J. Electrochem. Soc.* **145,** 3392 (1998).
18. R. Giovanoli, E. Stähli, and W. Feitknecht, *Helv. Chim. Acta* **53,** 209 (1970).
19. S. Hirano, R. Narita, and S. Naka, *Mater. Res. Bull.* **19,** 1229 (1984).
20. G. Pistoia, G. Antonini, D. Zana, and M. Pasquali, *J. Power Sources* **56,** 37 (1995).
21. Y. Xia, H. Noguchi, and M. Yoshio, *J. Solid. State. Chem.* **119,** 216 (1995).
22. P. Ruetschi, *J. Electrochem. Soc.* **131,** 2737 (1984).
23. P. Ruetschi and R. Giovanoli, *J. Electrochem. Soc.* **35,** 2663 (1988).
24. Y. Chabre and J. Pannetier, *Prog. Solid State. Chem.* **23,** 1 (1995).
25. H. Abbas, Kh. Abou-El-Sherbini, M. Askar, and A Hashim, *J. Mater. Sci. Technol.* **17,** 351 (2001).
26. Kh. Abou-El-Sherbini, M. Askar, and R. Schöllhorn, *J. Solid State Ionics*, in press.
27. P. Chatterjee, *J. Appl. Polym. Sci.* **12,** 1859 (1968).
28. L. MacLean, Ch. Poinsignon, J. Amarilla, F. Le Cras, and P. Strobel, *J. Mater Chem.* **5,** 1183 (1995).
29. R. Potter and G. Rossman, *Am. Miner.* **64,** 1199 (1979).
30. T. Ohzuku, I. Tari, and T. Hirai, *Electrochimi. Acta* **27,** 1049 (1982).